Mathematical Biosciences 372 (2024) 109192

Contents lists available at ScienceDirect

Mathematical Biosciences

journal homepage: www.elsevier.com/locate/mbs

Original Research Article

Modeling realistic synaptic inputs of CA1 hippocampal pyramidal neurons and interneurons via Adaptive Generalized Leaky Integrate-and-Fire models

A. Marasco [a,b,*], C. Tribuzi [a], C.A. Lupascu [b], M. Migliore [b]

[a] Department of Mathematics and Applications, University of Naples Federico II, Naples, Italy
[b] Institute of Biophysics, National Research Council, Palermo, Italy

ARTICLE INFO

Keywords:
Neuronal modeling
Generalized leaky integrate-and-fire models
Large-scale neuronal network
Hippocampal CA1 pyramidal neurons and interneurons
Synaptic inputs

ABSTRACT

Computational models of brain regions are crucial for understanding neuronal network dynamics and the emergence of cognitive functions. However, current supercomputing limitations hinder the implementation of large networks with millions of morphological and biophysical accurate neurons. Consequently, research has focused on simplified spiking neuron models, ranging from the computationally fast Leaky Integrate and Fire (LIF) linear models to more sophisticated non-linear implementations like Adaptive Exponential (AdEX) and Izhikevic models, through Generalized Leaky Integrate and Fire (GLIF) approaches. However, in almost all cases, these models are tuned (and can be validated) only under constant current injections and they may not, in general, also reproduce experimental findings under variable currents. This study introduces an Adaptive GLIF (A-GLIF) approach that addresses this limitation by incorporating a new set of update rules. The extended A-GLIF model successfully reproduces both constant and variable current inputs, and it was validated against the results obtained using a biophysical accurate model neuron. This enhancement provides researchers with a tool to optimize spiking neuron models using classic experimental traces under constant current injections, reliably predicting responses to synaptic inputs, which can be confidently used for large-scale network implementations.

1. Introduction

Full-scale computational models of brain regions are a fundamental tool to investigate the dynamics of neuronal networks and the emergence of cognitive functions. Unfortunately a morphological and biophysical accurate implementation of large networks in the order of millions of neurons is beyond the technical possibilities of the current supercomputing systems. For this reason, the research in this field has been more and more focused on simplified neuron models, to find the simplest way to reproduce the firing behavior of different neuronal population. This is an important step, since it will drastically reduce the computational resources needed to carry out simulations of brain regions at full-scale cellular-level implementation, composed of million of neurons and billions of synapses. A number of conceptually different approaches are currently used, from the computationally fast and extremely simplified, Leaky Integrate and Fire (LIF) linear models (see [1,2]), to more sophisticated, non-linear implementations such as Adaptive Exponential (AdEX) [3,4] and Izhikevic models (see [5,6]). The use of a linear system in any LIF-type model allows a full mathematical analysis of the parameters' space, which is instrumental in finding the ensemble of update rules and constraints needed to quantitatively reproduce all the observed experimental firing behaviors. However, all LIF models with constant initial conditions and update rules cannot mathematically describe even the simplest typical nonlinear dynamics of CA1 neurons, such as adaptation. A different approach to simulate the neuron dynamics in the presence of synaptic inputs is to replace the solution of a nonlinear model with event-driven-lookup-tables (ED-LUT) of precalculated function values (see [7,8]). However, when applied to large networks, it requires to store a prohibitively large volume of data.

Recent advances include implementations of Generalized Leaky Integrate and Fire (GLIF) models (see [9–12]), in which the linear system of ODEs is complemented by an appropriate set of initial data and updating rules that effectively introduce the non-linear behavior in the voltage dynamics observed in real neurons. In a previous work [13], we introduced an adaptive generalized leaky integrate-and fire model for hippocampal CA1 neurons and interneurons, in which the nonlinear nature of the firing dynamics is successfully reproduced by employing nonlinear and more realistic initial and update conditions after each spike event, which strictly depends on the external stimulation current.

* Corresponding author at: Department of Mathematics and Applications, University of Naples Federico II, Naples, Italy.
E-mail address: marasco@unina.it (A. Marasco).

https://doi.org/10.1016/j.mbs.2024.109192
Received 21 December 2023; Received in revised form 14 March 2024; Accepted 9 April 2024
Available online 17 April 2024

Moreover, we have recently demonstrated in [14] that, using the A-GLIF approach, it is possible to create an unlimited replica of spiking neuron models of hippocampal pyramidal neurons and interneurons, in quantitative agreement with over 300 experimental recordings under constant somatic current injections, and also reproducing the physiological variability. One limitation of such systems is that the resulting models can be validated only under the experimental protocols used for the optimization procedure, which almost exclusively consist of constant somatic current injections. Because of the intrinsic simplified mathematical structure, any given LIF-based spiking neuron model cannot, in general, also reproduce experimental traces under variable current injections (such as that generated by synaptic inputs). This is particularly evident in a recent work [11] where a GLIF implementation was used to generate models of experimental data obtained under dynamic clamp conditions, using fitting-tools and post-hoc optimization procedures based on a set of training stimuli such as short and long square, and noisy stimuli. Although these models were able to be qualitatively consistent with many experimental recordings, their performance in reproducing traces obtained under constant current injections was rather poor. In this paper we show how to solve this limitation by extending our A-GLIF model with a new set of update rules that make a neuron model able to reproduce both constant and variable current inputs. We tested the performances and the accuracy of the results under a variety of conditions, using as a reference the responses of a biophysical and morphological accurate model neuron to synaptic inputs, activated following natural patterns recorded from 10 presynaptic neurons during in vivo exploratory behavior. This work will allow a researcher to confidently optimize a spiking neuron model using a "classic" set of experimental traces under constant current injections to implement a model that will also predict the response to a barrage of synaptic inputs.

2. Materials and methods

2.1. Reference model traces in response to synaptic inputs

All simulations relative to the reference hippocampal CA1 pyramidal neuron model were carried out using the NEURON simulator (v8.0.0) [15], whereas simulations with the A-GLIF model were implemented in Python (see Section 2.5). For the reference neuron simulations, we used a 3D reconstruction of a rat hippocampus CA1 pyramidal neuron (morphology oh140807_A0_idB.asc from https://zenodo.org/api/files/e01bb8ba-976f-4506-8c83-ccdce2161893/oh140807_A0_idB.ASC).

The passive properties were consistent with those measured in CA1 pyramidal neurons (Cm = 1 μF/cm^2, Rm = 30,000 Ω/cm^2), with a resting potential set to −70 mV. For the purpose of this paper, and to reduce computational resources and energy consumption, active conductances (including a Sodium channel, a delayed rectifier (KDR), and a KV7 (KM) Potassium channels, from [16] were included only in the soma; their peak values were adjusted to be consistent with the firing properties of a typical CA1 pyramidal neuron; the equations describing each channel kinetics are described elsewhere (see [17]).

To obtain from the reference neuron a set of responses to synaptic stimulations similar to the in-vivo conditions, we placed a synaptic input in the soma, effectively representing the overall somatic response to a volley of afferent Schaeffer Collaterals synapses. It was implemented as a double exponential current (with 0.5 and 20 ms of rise and decay time constant, respectively), and activated using a set of preSynaptic Activation Times (pSAT 1-10) corresponding to the spike times recorded during open-field explorations recorded in vivo from 10 CA3 pyramidal neurons of male Long-Evans rats (300–500 g), as described in [18]. This allowed to use very realistic synaptic input patterns, instead of rather artificial random stimulations, to test our models.

A raster plot representing the pSATs of all the 10 CA3 neurons is reported in Fig. 1A, and demonstrates the wide variability of the synaptic activation times that a CA1 pyramidal neuron can experience during 10 min of a typical in vivo behavior. To model a physiologically plausible variability in the synaptic strength, we used a wide range of peak synaptic currents. From now on, the current generated by each pSAT will thus be identified as Synaptic Activation Pattern (SAP), each one associated with a given peak synaptic current. A simulation campaign was carried out by using values in the range 50–1250 pA with a step of 100 pA. A few representative SAPs generated on the CA1 neuron soma by the corresponding pSAT, using peak synaptic weights of 450 and 1250 pA, are plotted in Fig. 1B (top plots) (Fig. 1), together with the resulting somatic voltage in the reference CA1 pyramidal neuron model (see Fig. 1B bottom plots).

In Fig. 2 we schematically illustrate the simulation setup for the reference neuron, during three 2-s time windows of the pSAT-1 pattern (Fig. 2, left). The arrow and the electrode in the middle panel of Fig. 2 indicate the injection and recording locations in the reference neuron, respectively. The somatic responses to the three streams, with a 450 pA peak value, highlight the wide variability of the interspike intervals during an in vivo activity (Fig. 2, right, top three traces). The synaptic input current generated by the red input train is shown in the right panel of Fig. 2, right (bottom trace).

2.2. The A–GLIF model for constant and piecewise constant stimulation currents

In [13] we introduced the A-GLIF model, to describe the dynamics, in a subthreshold regime, of the membrane (somatic) potential V in response to *constant current injections*. The model is written in terms of a system of three linear ordinary differential equations (ODEs) representing the evolution of the potential V and two intrinsic currents I_{adap} and I_{dep} as follows:

$$\begin{aligned} \frac{dV}{dt} &= \frac{1}{C_m}\left[\frac{C_m}{\tau_m}\left(V - E_L\right) - I_{adap} + I_{dep} + I_{stim}\right], \\ \frac{dI_{adap}}{dt} &= -k_2 I_{adap} + C_m k_1 k_2 \left(V - E_L\right), \\ \frac{dI_{dep}}{dt} &= -k_1 I_{dep}, \end{aligned} \tag{1}$$

where all parameters are positive, except for the resting potential E_L, and the injected current I_{stim} which can also be negative (see Table 1). In (1) the adaptation current I_{adap} simulates the activation of the outward currents causing a hyperpolarizing effect, whereas the depolarizing current I_{dep} represents inward currents.

Despite the linearity of the equations, the A-GLIF model is able to reproduce a wide range of physiological firing patterns like bursting, non adapting, and continuous adapting provided that it is equipped with suitable nonlinear initial and update conditions after each spike event, which strictly depend on the external stimulation current (see [13]).

Let I_{th} be the *threshold current* above which the neuron starts to fire, i.e. we suppose that a spike event occurs when, for $I_{stim} > I_{th}$, the potential V reaches the *threshold potential* V_{th}. Moreover, we assume that the neuron is at rest for $t < t_{start}$, i.e. $I_{stim} = 0$ and $V = E_L$, where t_{start} is the last instant in which $I_{stim} = 0$.

Starting from the resting condition, the *first spike*, for any constant stimulation current I_{stim} : $I_{stim} > I_{th}$, can be obtained by setting the initial conditions of the Cauchy problem associated to system (1) as follows

$$\begin{aligned} V(t_{start}) &= E_L, \\ I_{adap}(t_{start}) &= 0, \\ I_{dep}(t_{start}) &= I_{dep}^{start}(I_{stim} - I_{th})\,\theta(I_{stim} - I_{th}), \end{aligned} \tag{2}$$

where I_{dep}^{start} is a suitable constant and $\theta(I_{stim} - I_{th})$ is the step function defined as

$$\theta(I_{stim} - I_{th}) = \begin{cases} 1 & \text{if } I_{stim} > I_{th}, \\ 0 & \text{if } I_{stim} \le I_{th}. \end{cases} \tag{3}$$

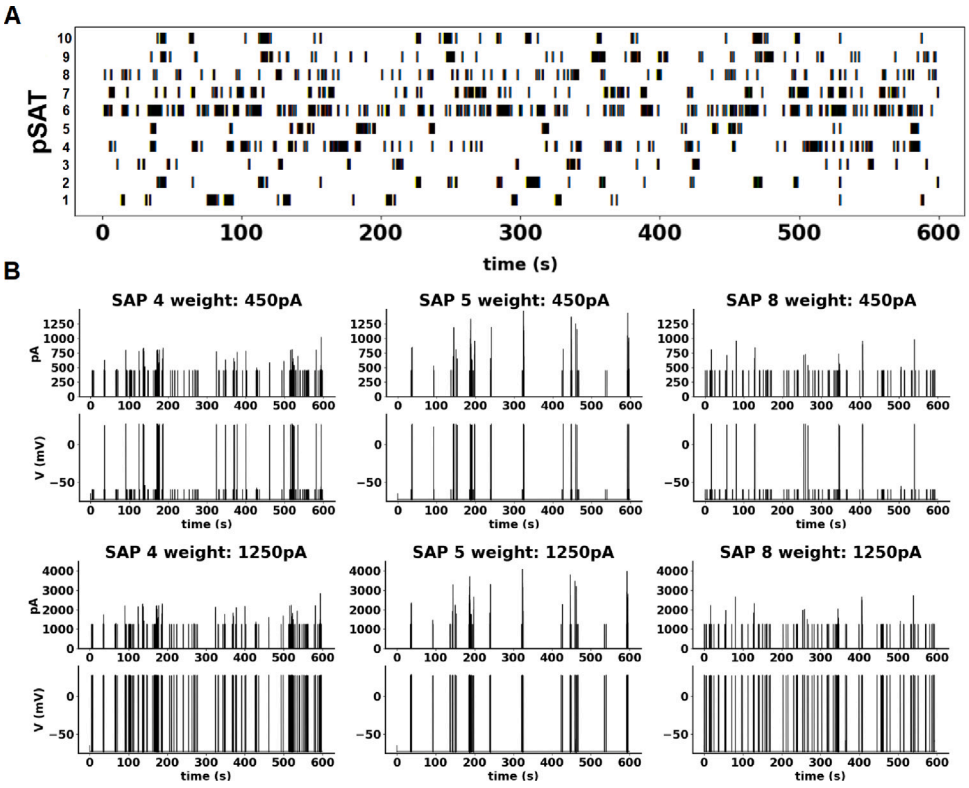

Fig. 1. Input patterns. (A) Typical raster plots (top) of the presynaptic spike times (pSAT) recorded from 10 individual rat CA3 pyramidal cells during 10 min open-field exploration. (B) Typical synaptic activation patterns (SAPs) in response to different pSATs with different weights. (Left, top panel) The current (top) and the corresponding somatic response (bottom) generated by pSAT 4 with a peak synaptic current of 450 pA; (Left, middle panel); current (top) and somatic response (bottom) generated by pSAT 4 with a peak synaptic current of 1250 pA; (Middle and right) Same as for left panels but using pSAT 5 and pSAT 8.

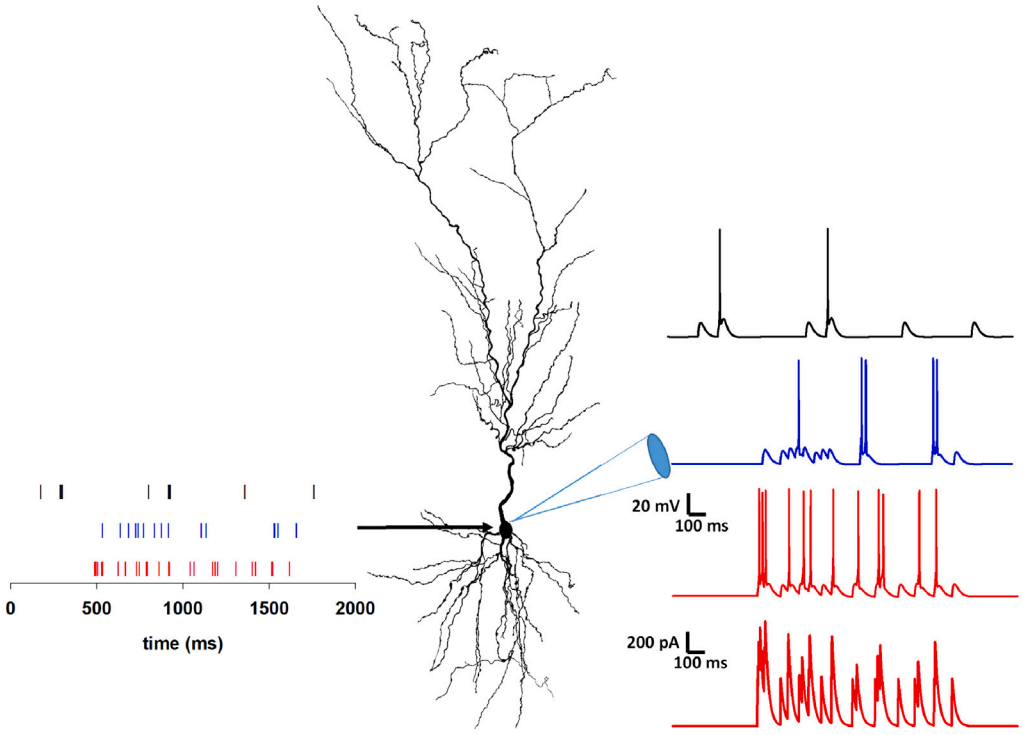

Fig. 2. Schematic setup of the simulation campaign. (Left) Typical 2-s windows of experimental spike times recorded from CA3 pyramidal neurons (from pSAT 1), recorded during 10 min sessions of *in vivo* exploration [18]. They were used to activate an excitatory synapse on the soma of a CA1 pyramidal neuron (middle). On the right, we shown the somatic membrane in response to the three patterns (black, blue, and red traces, from SAP 1 with weight 450 pA, and one example of the synaptic current generated by the red train (bottom trace on the right).

Table 1
List of parameters appearing in Eq. (1) including their description and measurement unit.

Parameter	Description	UM
E_L	Resting potential for $I_{stim} = 0$	mV
V_r	Reset potential	mV
V_{th}	Threshold potential	mV
Δt_{ref}	Refractory interval	ms
I_{stim}	External stimulation current	pA
C_m	Membrane capacitance	pF
τ_m	Membrane time constant	ms
I_{th}	Threshold stimulation current	pA
k_2	I_{adap} decay rate	ms^{-1}
k_1	I_{dep} decay rate	ms^{-1}

Following a LIF framework, the potential V after a spike does not return to the resting value E_L but at the *reset potential* V_r. Then, for any following spike, the initial conditions of each Cauchy problem for (1) are modified according to the following *after-spike update rules*

$$\begin{aligned} V(t_{spk}^+) &= V_r, \\ I_{adap}(t_{spk}^+) &= I_{adap}^0(t_{spk}^+, I_{stim}), \\ I_{dep}(t_{spk}^+) &= I_{dep}^0, \end{aligned} \tag{4}$$

where t_{spk}^+ is the time instant following the spike time t_{spk}, i.e. $t_{spk}^+ = t_{spk} + \Delta t_{ref}$, with $\Delta t_{ref} = 2\,\text{ms}$ representing the *refractory time*, I_{dep}^0 is a constant, and finally $I_{adap}^0(t_{spk}^+, I_{stim})$ is a Monod-type function that depend on both the stimulation current I_{stim} and the corresponding spike times as follows

$$I_{adap}^0(t_{spk}^+, I_{stim}) := S\left(c + \frac{a\, e^{b\, I_{stim}}\,(t_{spk}^+ - t_{start})}{d + (t_{spk}^+ - t_{start})}\right), \tag{5}$$

where $S = -E_L\, C_m k_1 > 0$, a, b, c, d are suitable constants ensuring that the function exists and is positive for all $I_{stim} > I_{th}$ and $t_{spk}^+ \in \left[t_{spk}^{first}\left(I_{stim}\right) - t_{start}, t_{spk}^{last-1}\left(I_{stim}\right) - t_{start}\right]$, where t_{spk}^{first} (resp. t_{spk}^{last-1}) is the time of the first (resp. second-last) spike event for the current I_{stim}.

In [13] we derived the sufficient conditions on the parameters a, b, c, d which ensure the existence and positivity of the function (5). We note that Eq. (5) defines a sequence of *constant ISIs* when $a = 0$ and $c \geq 0$ or $d = 0$ and $c + a\exp(b\, I_{stim}) > 0$. Furthermore, assuming $a \neq 0$ and $d > 0$, we obtain a sequence of *nonconstant ISIs* when the following conditions hold

(i) either $a > 0, \quad c \geq 0, \quad \forall b,$
(ii) or $a < 0, \quad b < 0, \quad c \geq -a.$

Moreover, to reproduce the *firing block*, i.e. the event in which a neuron stops firing long before the end of the stimulation, in [13] was implemented the Monod block procedure that allowed us to determine the time interval

$$[t_{spk}^{first}\left(I_{stim}\right) - t_{start},\, t_{block}\left(I_{stim}\right)], \quad \forall I_{stim} > I_{th} \tag{6}$$

in which the function (5) should be defined.

In [13] we performed a nondimensional analysis of the model (1) that allows (i) to reduce the number of parameters and consequently to obtain a general integral easier to analyze, and (ii) to determine general constraints on model's parameters through both the stability analysis of the equilibria and the study of the monotonicity properties of the membrane potential w.r.t. model parameters (see Appendix A.1 in the Supporting information).

Moreover, assuming a *constant stimulation current* I_{stim}, we obtained the analytical form of the solutions of the nondimensional version of system (1) (see Eq. (26)). We note that when we take into account a *constant piecewise injected current*, all the qualitative and quantitative results on the equilibria, solutions, and parameter constraints still hold in each interval in which the current remains constant. However, owing to the discontinuities in the injected current, to accurately reproduce the dynamical behavior of the membrane potential in the presence of piecewise constant current, the model need to be equipped with additional initial and update rules to take into account the current changes. To ensure that the model would also be able to predict the neuron dynamics (and in particular the spike times) both for constant currents outside the experimental range (used for the optimization process) and for piecewise constant stimulation currents, in [13], we introduced the updates rules (34)–(39) reported in Appendix A.2 of the Supporting information.

2.3. The A-GLIF model for synaptic inputs

In presence of time-varying stimulation currents ($I_{stim} = I_{stim}(t)$) system (1) cannot admit a general integral in a closed form. Consequently, both the analytical solutions and all the stability and monotonicity properties of the membrane potential, as reported in Appendix A.1 of the Supporting information, are no longer valid. Furthermore, if we try to numerically integrate the A-GLIF model (1) in the presence of an arbitrary synaptic input ($I_{stim} = I_{stim}(t)$ and without any additional condition, apart from those described in Appendix A.2 of the Supporting information (see Eq. (34)–(39)), we obtain a dynamical behavior of the membrane potential which is far from reproducing the real neuronal activity. This problem can be appreciated in Fig. 3, where we show a typical pSAT (top plot), the corresponding voltage response in the full neuron (Fig. 3, "in silico" plot), the response of the original A-GLIF model (Fig. 3, "ODE" plot), compared with the response obtained with the update rules presented in this work (see Fig. 3, "model" plot).

From a mathematical point of view, to obtain a model able to reproduce the correct somatic voltage dynamics under any stimulation protocol it is necessary to suitably modify both the equations in (1) and the initial data in (2) and (4).

For this purpose, we determined few additional initial conditions and update rules preserving both the analytical solutions (26) and all the results obtained from the qualitative analysis. In detail, in the presence of time-dependent stimulation currents ($\alpha = \alpha(t)$), instead of the nondimensional system (22) we consider the following *nonautonomous* system

$$\frac{dV}{dt} = \alpha(t) + \beta(I_{dep} - I_{adap}) + \delta(1 + V) + F(t), \tag{7a}$$

$$\frac{dI_{adap}}{dt} = 1 - I_{adap} + V + G(t), \tag{7b}$$

$$\frac{dI_{dep}}{dt} = -\beta I_{dep}, \tag{7c}$$

where

$$\begin{aligned} G(t) &= \frac{1}{2(\beta - \delta)}\left[2 + (\delta - 1)\mathcal{H}_1 - \mathcal{H}_2\right]\alpha'(t), \\ F(t) &= G(t) + \mathcal{H}_1\alpha'(t), \end{aligned} \tag{8}$$

and $\mathcal{A}, \mathcal{B}(t), C(t), \mathcal{H}_1(t), \mathcal{H}_2(t)$ are defined in (28).

System (7) is obtained by imposing that the explicit solutions (26) determined in the case of constant α are preserved as solutions of its extension for $\alpha = \alpha(t)$. This allows to preserve the results obtained from the stability analysis also for a variable current regime. As the presence of this time-dependent parameter does not affect the dynamics of I_{dep}, Eq. (7c) coincides with Eq. $(22)_3$. Instead, the additional terms that must be included in Eqs. $(22)_{1,2}$, to satisfy this constraint, correspond to the functions in (8). Due to their dependence on $\alpha'(t)$, in the case of a constant stimulation current these functions vanish and the system (7) coincides with (22), ensuring the mathematical consistency of our framework.

We note that, as in the case of constant or piecewise constant stimulation currents, the initial and update conditions (25), require additional modifications to reproduce all the experimental traces obtained under synaptic currents. In the following, we complement these rules to make the model able to reproduce the voltage dynamics in response to an arbitrarily variable input current, such that generated in a network.

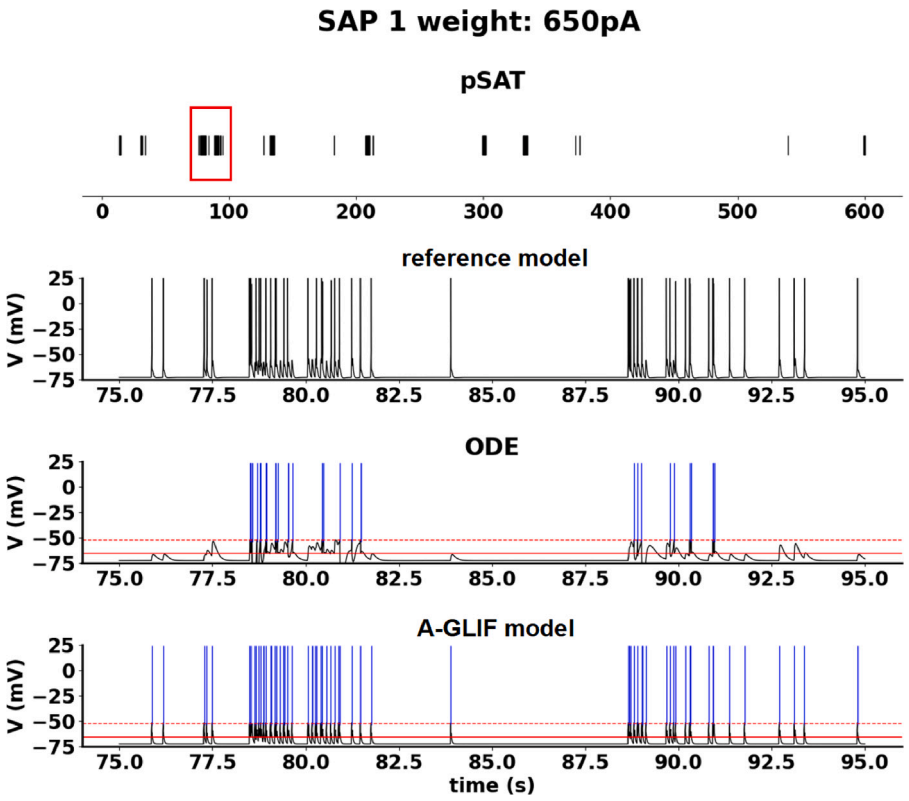

Fig. 3. Any LIF or GLIF system tuned to constant current injections cannot be assumed to also reproduce the response to synaptic inputs. (top) Raster plot for pSAT-1 during a 600 s long recording period; (reference model) Somatic voltage trace from a simulation of the reference model in the interval 75–95 s; (ODE): model trace obtained by numerical integration of the A-GLIF model (1) with $I_{\text{stim}} = I_{\text{stim}}(t)$ and initial and update conditions (2)–(4); (A-GLIF model): dynamics of the membrane voltage (26) with $I_{\text{stim}} = I_{\text{stim}}(t)$ equipped with initial and update conditions for $V^0, I^0_{\text{adap}}, I^0_{\text{dep}}$ as defined in Sections 3 and A.2. Blue bars represent spike times, whereas red dashed and continuous lines represent V_{th} and V_{r}, respectively.

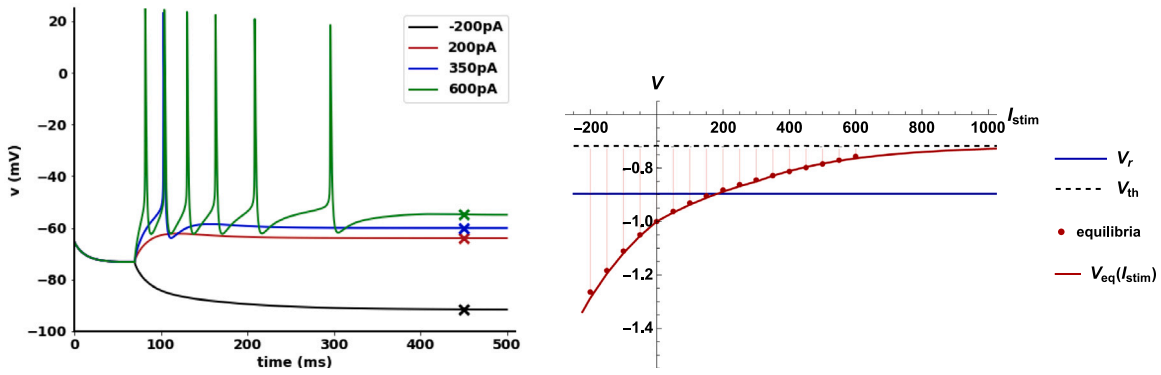

Fig. 4. (left) Reference model traces, the cross markers represent voltage equilibria. (right) Function (9) interpolating the voltage equilibria, black dashed and blue lines represent V_{th} and V_r, respectively.

4. The first property that we need to consider is the voltage dynamics after a burst of spikes and also when the neuron never fires (i.e. $I_{\text{stim}} < I_{\text{th}}$). Experimentally, it can be observed that the voltage reaches a steady-state that depends on both the input current and the past spiking activity. This effect can be appreciated in Fig. 4 (top plots), where we show some typical examples obtained in our reference model for constant currents of −200, 200, 350, and 600 pA. In Fig. 4 we plot the steady-state value as a function of the input current (red points). As can be seen, the values appears to be along an exponential-type curve. However, we found they cannot be adequately fitted with a single function (not shown). This is probably due to the different ion channels state and dynamics in the different input current regimes (hyperpolarized, subthreshold, and suprathreshold). In order to introduce how we considered these conditions, we proceeded as follows. Let t be a time such that $I_{\text{stim}}(t) < I_{\text{th}}$ or $I_{\text{stim}}(t) \geq I_{\text{th}}$ but $t \geq t_{\text{block}}(I_{\text{stim}})$, where t_{block} is the time of the last spike before the silent period (i.e. the last instant in which the Monod function exists). Then, in these cases there are no spikes and the voltage reaches an equilibrium state defined by the following nondimensional function

$$V_{\text{eq}}(I_{\text{stim}}) = \begin{cases} V_{\text{min}} & \text{if } I_{\text{stim}} < I^{\text{neg}}_{\text{stim}}, \\ V_{\text{th}} - e^{-\xi I_{\text{stim}}}(V_{\text{th}} - E_{\text{L}}) & \text{if } I^{\text{neg}}_{\text{stim}} \leq I_{\text{stim}} \leq 0, \\ V_{\text{th}} - e^{-\eta I_{\text{stim}}}(V_{\text{th}} - E_{\text{L}}) & \text{if } 0 < I_{\text{stim}} \leq I_{\text{th}}, \\ V_{\text{th}} - e^{-\zeta I_{\text{stim}} + \rho I_{\text{th}}}(V_{\text{th}} - E_{\text{L}}) & \text{if } I_{\text{stim}} > I_{\text{th}}, \end{cases} \tag{9}$$

where $V_{\min}$ is the nondimensional value of the minimum physiologically plausible voltage, corresponding to the reversal potential of potassium currents (e.g. $= -90\,\mathrm{mV}$), $I_{\mathrm{stim}}^{\mathrm{neg}}$ is the (experimentally measured) current for which the cell relaxes to $V_{\min}$, and finally ξ, η, ζ, ρ are nonnegative constant that must be determined through an optimization procedure. Furthermore, by imposing that the function (9) is continuous for $I_{\mathrm{stim}} = I_{\mathrm{th}}$ we obtain the following constraint on the parameters $\eta = \zeta - \rho$. Then, for each interval, it would be sufficient to know only one experimental steady-state voltage to determine its value for any current.

For our reference model, $I_{\mathrm{stim}}^{\mathrm{neg}} = -185\,\mathrm{pA}, \xi = \zeta = 3.5 \cdot 10^{-3}, \eta = 2.5 \cdot 10^{-3}, \rho = 10^{-3}$. The corresponding curves are depicted in Fig. 4 (red line in the bottom plot).

5. Let t be a time such that $I_{\mathrm{stim}}(t - dt) < I_{\mathrm{th}}$ and $I_{\mathrm{stim}}(t) > I_{\mathrm{th}}$, then the system evolves starting from the following initial conditions

$$\begin{aligned} &V^0(t) = V_{\mathrm{eq}}(I_{\mathrm{stim}}(t)), \quad I_{\mathrm{adap}}^0(t) = 0, \\ &I_{\mathrm{dep}}^0(t) = \max\left(I_{\mathrm{dep}}^{\mathrm{start}}(I_{\mathrm{stim}}(t) - I_{\mathrm{th}})\theta(I_{\mathrm{stim}}(t) - I_{\mathrm{th}}), I_{\mathrm{dep}}^0\right), \end{aligned} \tag{10}$$

and the value of t_{start} is thus updated at the current instant t.

2.4. Statistical analysis and performance measures

To statistically verify that the A-GLIF model was able to reproduce the spike trains in response to any given synaptic stimulation pattern we relied on the *Mann–Whitney U-test* for univariate samples using the buit-in function `MannWhitneyTest` of the software Mathematica (ver. 13.01, Wolfram). For each of the 130 synaptic stimulations within the physiological range of input (i.e., below the depolarization block state, and up to a weight of 1.25 in our case) we considered the paired samples $\mathrm{data_E}$ (experimental data) and $\mathrm{data_M}$ (model data) of length n and m, respectively, as follows

$$\mathrm{data_E} = \{t_1, \dots, t_n\}, \qquad \mathrm{data_M} = \{\bar{t}_1, \dots, \bar{t}_m\}, \tag{11}$$

We performed the test only for the paired samples such that $n, m > 10$, and we tested the null hypothesis $H_0 : \mu_E = \mu_M$ against the alternative hypothesis $H_a : \mu_E \neq \mu_M$, where μ_E and μ_M are the median of the two data sets. For all data set the null hypothesis H_0 was rejected only if $p < \gamma$, where the significance level γ was set to 0.05.

Moreover, we tested whether the A-GLIF model was able to correctly identify the presence (or absence) of a spike within a given time interval. To this aim, for each of the 130 synaptic stimulation protocols, we calculated the following performance measures [19,20]

$$\begin{aligned} &\mathrm{Accuracy} = \frac{\mathrm{TP} + \mathrm{TN}}{\mathrm{TP} + \mathrm{FP} + \mathrm{TN} + \mathrm{FN}}, \quad \mathrm{Precision} = \frac{\mathrm{TP}}{\mathrm{TP} + \mathrm{FP}}, \\ &\mathrm{Recall} = \frac{\mathrm{TP}}{\mathrm{TP} + \mathrm{FN}}, \quad \mathrm{F-score} = \frac{2\mathrm{TP}}{2\mathrm{TP} + \mathrm{FP} + \mathrm{FN}} \end{aligned} \tag{12}$$

where TP (True Positives), is the number of spikes from the experimental trace that are also found in the A-GLIF model; TN (True Negatives) is the number of intervals in which the neuron does not fire a spike in both the reference and the A-GLIF models; FP (False Positives) is the number of mismatched spikes in the A-GLIF model; FN (False Negatives) is the number of spikes in the reference model that are not matched in the A-GLIF model.

The Accuracy takes into account how accurately the A-GLIF model reproduces both spiking and silent periods of the reference model. A value of 1 represents the ideal case of a perfect correspondence of spikes and silent periods between the reference and the A-GLIF models. Furthermore, all the other performance measures (11) do not consider silent periods, except for mismatched spike events within these periods (FP). Since all the quantities in (12) represent probability measures within a given time interval, their values may depend on the number of events occurring during simulations of different length. For all calculations we used the entire time interval of 600 s. In detail, the Precision represents the fraction of relevant spike times among all the retrieved spike times, whereas Recall is the fraction of relevant spike times that were retrieved. Finally, the F-score is the harmonic mean of the Precision and Recall measures.

Let N be the number of spikes in the reference model in the interval $[t_0, T]$. For any spike in the reference model at time t_i, TP, FP, and FN were calculated by exploring the behavior of the A-GLIF model in the time window

$$I(t_i) = \left[t_i - \omega(t_i - t_{i-1}), t_i + \omega(t_{i+1} - t_i)\right], \quad i = 1, \dots, N \tag{13}$$

where $t_{N+1} = T$, and $0 < \omega \leq 1/2$ to avoid overlaps between consecutive intervals (13), in such a way that

$$\mathrm{TP} = \begin{cases} 1 & \text{if there is at least 1 spike in the A-GLIF model,} \\ 0 & \text{otherwise,} \end{cases} \tag{14}$$

$$\mathrm{FP} = \begin{cases} n - 1 & \text{if there are } n > 1 \text{ spikes in the A-GLIF model,} \\ 0 & \text{otherwise,} \end{cases} \tag{15}$$

$$\mathrm{FN} = \begin{cases} 1 & \text{if there are no spikes in the A-GLIF model,} \\ 0 & \text{otherwise.} \end{cases} \tag{16}$$

It should be stressed that, in contrast with the conventional way to calculate these quantities, here we are using a variable time window (13), which is adapted to follow the instantaneous firing behavior. Moreover, to take into account long silent intervals, the maximum amplitude $A_i = \omega(t_{i+1} - t_{i-1})$ of any interval (13) was set to 2Λ. In detail, when $\omega(t_i - t_{i-1})$ and/or $\omega(t_{i+1} - t_i)$ are greater than Λ, we modify the intervals (13) as follows (see gray regions in Fig. 5)

$$I(t_i) = \left[t_i - \varphi_i, t_i + \varphi_{i+1}\right], \quad i = 1, \dots, N \tag{17}$$

where

$$\varphi_i = \begin{cases} \omega(t_i - t_{i-1}), & \text{if } \omega(t_i - t_{i-1}) \leq \Lambda, \\ \Lambda, & \text{otherwise,} \end{cases} \tag{18}$$

and, according to the literature, Λ could range from 10 ms to 1s (see [21]).

To calculate TN and any other FP, we consider the following intervals where there is no activity in the reference model (see light blue regions in Fig. 5)[1]

$$\begin{aligned} &\tilde{I}(t_0) = \left[t_0, t_1 - \omega(t_1 - t_0)\right], \\ &\tilde{I}(t_i) = \left[t_i + \omega(t_{i+1} - t_i), t_{i+1} - \omega(t_{i+1} - t_i)\right], \quad i = 1, \dots, N-1, \\ &\tilde{I}(t_N) = \left[t_N + \omega(t_{N+1} - t_N), t_{N+1}\right]. \end{aligned} \tag{19}$$

Finally, to evaluate the FP relative to the intervals (19) we use the following rule

$$\mathrm{FP} = \begin{cases} n & \text{if there are } n \text{ spikes in the A-GLIF model,} \\ 0 & \text{otherwise,} \end{cases} \tag{20}$$

whereas TN is equal to the number M_i of subintervals of $\tilde{I}(t_i)$, of maximum amplitude Λ_i, without any spike in the A-GLIF model. In order not to overestimate the number of TNs in long silent intervals, the number M_i and the parameter Λ_i are determined as follows

$$M_i = \begin{cases} 1, & \text{if } \tilde{A}_i \leq 2\Lambda, \\ \left\lceil \dfrac{\tilde{A}_i}{2\Lambda} \right\rceil, & \text{if } 2\Lambda < \tilde{A}_i < 2c\,\Lambda, \\ \lceil c \rceil, & \text{otherwise,} \end{cases} \qquad \Lambda_i = \frac{\tilde{A}_i}{M_i}, \tag{21}$$

where $\tilde{A}_i$ is the amplitude of each interval (19), $\lceil \cdot \rceil$ denote the ceiling function, and $c \geq 1$ is a suitable positive constant such that it results $1 \leq M_i \leq \lceil c \rceil$ for all $i = 0, \dots, N$.

[1] Owing to Eq. (18), the intervals $\tilde{I}(t_i)$ for $i = 1, \dots, N-1$ becomes $\tilde{I}(t_i) = \left[t_i + \varphi_{i+1}, t_{i+1} - \varphi_{i+1}\right]$.

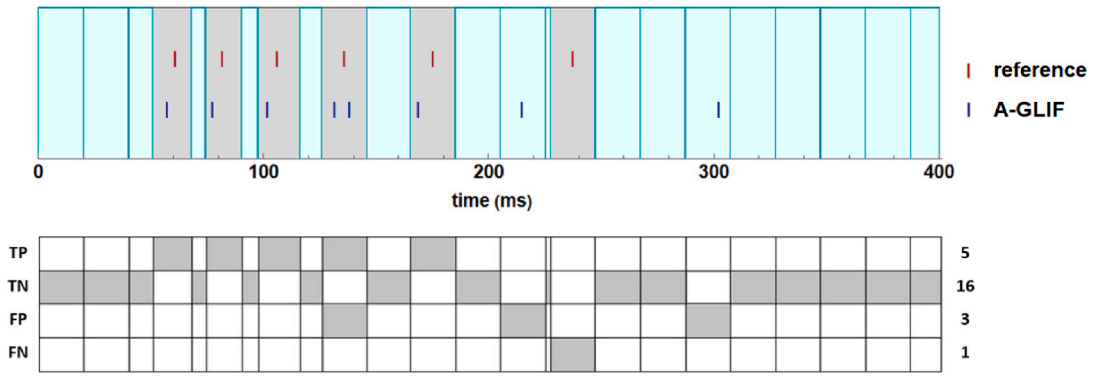

Fig. 5. Illustration of the calculation procedures of the performance measures (12). (Top) Raster plots representing spike times from reference (red bars) and A-GLIF (blue bars) models. Cyan and gray regions refer to intervals (13) and (19), respectively. (Bottom) The spike trains were scanned to test for mismatch of spikes or silent periods occurring within a variable time window as described in Section 2.4. Setting $\omega = 0.35$, $\Lambda = 10\,\text{ms}$, and $c = 10$, we obtain the following values of the performance measures: Accuracy = 0.84, Precision = 0.625, Recall = 0.83, F-score = 0.71.

The parameters ω, Λ, and c must be chosen appropriately for the given spike trains, considering both the time-scale of the spike events and their firing characteristics. Unless noted otherwise, in all simulations we used $\omega = 0.35$, $\Lambda = 10\,\text{ms}$, and $c = 10$. Considering that the in vivo activity of any given CA1 neuron includes long (in the order of seconds) silent periods, a maximum shift of ± 10 ms for the detection of true spike times in the time window (13) ensures a precise identification of spike occurrences.

An in-depth investigation on the performance metrics (12) will be conducted elsewhere, together with a comparison with different spike trains similarity measures reported in the literature (see [21–23]).

2.5. New A-GLIF model implementation and simulation codes

All model and simulation files relative to the reference model and the synaptic inputs are available in the ModelDB section of the Senselab database (https://modeldb.science/2015423). The numerical integration of the A-GLIF model as reported in Fig. 3 is implemented in NEST and is available in the ModelDB (https://modeldb.science/2015423).

The A-GLIF model is implemented starting from the following input data.

(a) The optimized parameters of the reference model generated by the optimization procedure, based on spike times in response to a set of constant currents injection, described in [13] and available in the ModelDB section of the Senselab database (https://modeldb.science/267598).
(b) The numerical values of the parameters ξ, η, ζ related to the voltage equilibrium function (9) (since $\rho = \zeta - \eta$) obtained from a set of simulations of the reference model as described in Fig. 4.

The A-GLIF model for synaptic inputs is implemented in Python, and the simulator source code is available in ModelDB (https://modeldb.science/2015423).

A schematic representation of the model implementation is outlined in Fig. 6.

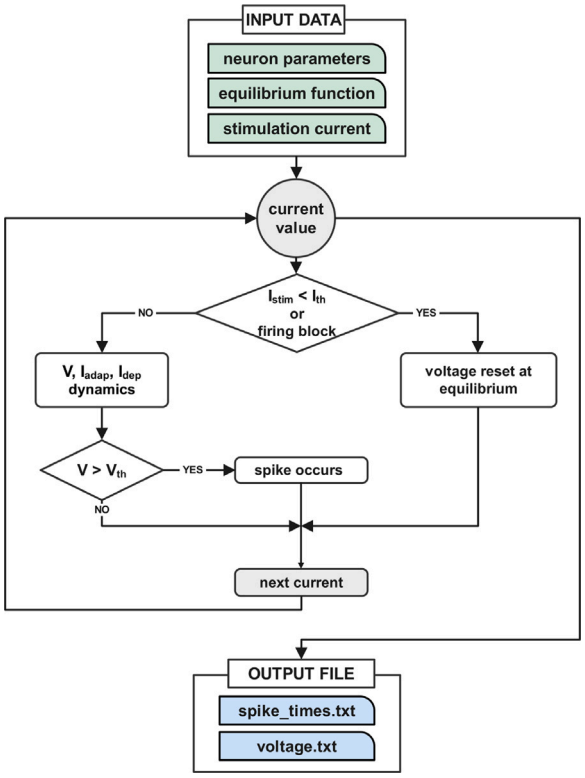

Fig. 6. Flow-chart illustration of the numerical implementation of the A-GLIF model for synaptic inputs. The input data contains (i) the neuron parameters resulting from the optimization procedure activated on constant stimulation currents, (ii) the parameters used to define the equilibrium function (9), (iii) and the list of the synaptic current values with a temporal step Δt. The code generates TXT files containing both spike times and voltage values at Δt steps.

3. Results

3.1. Reference responses to synaptic activation patterns

An overall picture of the wide range of variability that we considered in this work is illustrated in Fig. 7 (left), where we show the total number of spikes elicited by each SAP as a function of the peak synaptic weight. It should be stressed that each SAT represents a corresponding pSAT, which reproduces the in vivo presynaptic spike times of individual CA3 neurons during a 10 min period of exploratory behavior. Their activity depend on the specific role that each CA3 neuron has in the circuits involved in this behavior. As illustrated in Fig. 7 (right), using a peak synaptic weight of 750 pA, each SAT elicits a spiking pattern in our CA1 model neuron which includes a wide range of firing behavior, from the relatively regular tonic activity of SAP 6 (Fig. 7, right), to the rather systematic bursting activity exhibited by SAP 1 or SAP 3. We believe that these conditions represent a very good test of the flexibility and robustness of our approach.

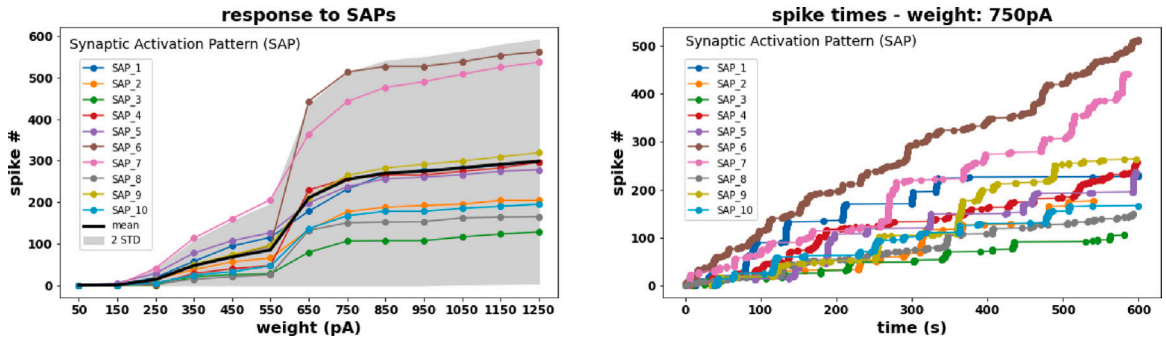

Fig. 7. The full set of results, obtained from the reference model simulations, that were used to test the A-GLIF model under a variety of synaptic inputs. (left) Total number of spikes generated by the different SAPs as a function of the synaptic weight. The thick black line represent the average values, and the gray area corresponds to ±2 SD. (right) Number of spikes generated as a function of time by the different SAPs (with a weight of 750 pA) during a 10 min simulation.

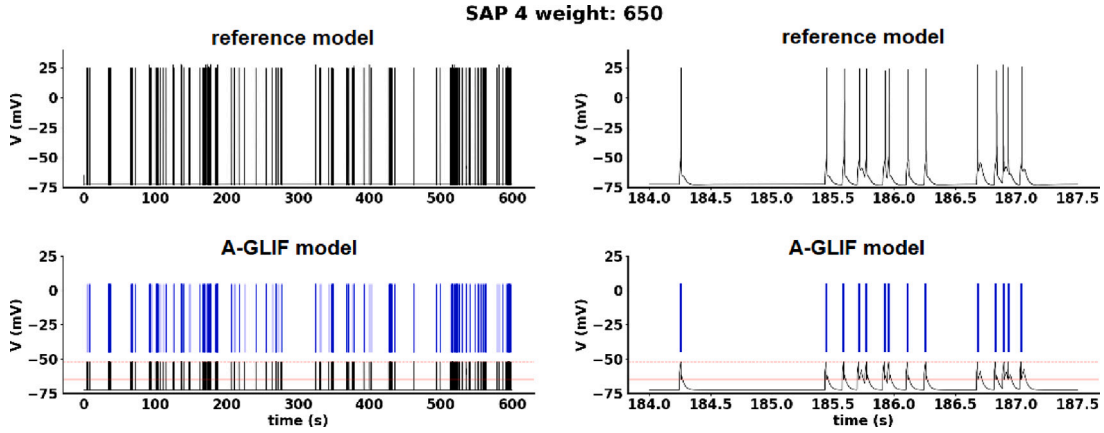

Fig. 8. Model validation for synaptic inputs. Top panels: (left) Reference model traces generated by the synaptic stimulation SAP 4 with a weight of 450 pA during a 10 min simulation. (right) Same as for the left but in the time interval 184–187.5 s. Bottom panels: A-GLIF model traces, blue bars represent spike times, whereas red dashed and continuous lines represent V_{th} and V_r, respectively.

3.2. Model validation under synaptic inputs

In [13] we optimized the A-GLIF model to reproduce the traces obtained with the reference model under constant stimulation currents, and validated the model on both constant and piecewise constant currents different from those used to optimize the model parameters. We also noted that the dynamical behavior of the membrane potential in the presence of piecewise constant currents was, in general, rather different from what can be observed for constant stimulation currents. These behaviors are caused by the nonlinear dynamics of the ion channel currents, which can be captured by a biophysical accurate model but it is out of reach for any GLIF model calibrated only on constant currents. For this reason, we also suggested further conditions to reproduce the dynamical behavior of the membrane potential in the presence of piecewise constant currents. In this paper, we complete the previous analysis by introducing an additional set of initial data (see Eq. (10)) able to reproduce the voltage dynamics in response to an arbitrarily variable input current, in such a way to consider the synaptic inputs activity that a given neuron can receive when embedded into a network. With suitable additional initial and update conditions (see Section 2.2–2.3), the A-GLIF model, previously optimized for constant current injections, is now automatically able to reproduce the response to any synaptic stimulation protocols. In Fig. 8 we compare the reference model traces (Fig. 8, top) with those obtained via the A-GLIF model (Fig. 8, bottom) for the synaptic stimulation generated by pSAT 4 with a peak synaptic current of 450 pA. The A-GLIF model allows for both accurately reproducing the excitability properties of the neurons and making the subthreshold dynamics of V more realistic compared to traditional LIF implementations. This is particularly evident in the right panel of Fig. 8, where the subthreshold relaxation of V from V_{reset} exhibits monotonicity properties consistent with the reference model but that are atypical for a classic LIF model.

The model was tested under the full set of 130 synaptic stimulation currents and, in all cases, the spike times observed in the reference and A-GLIF models were statistically indistinguishable as demonstrated in Table A.1, where it was $p > 0.05$ for all stimulations. As a further demonstration of the goodness of the model results, we calculated four different performance metrics: Accuracy, Precision, Recall, and F-Score; their definition in terms of TP, TN, FP, and FN are reported in Section 2.4, and the results are presented in Fig. 9, using different color schemes for each plot to stress that they refer to different metrics. A value of 1 for the Accuracy represents the best-case scenario of a perfect match of spikes and silent periods between the reference and the A-GLIF models. As can be seen, the Accuracy (Fig. 9, top left) ranges from 0.878 (e.g. SAP 5, weight 1250 pA) to 1.0, with a mean value of 0.958 over the entire set of simulations. Lower values of accuracy were found especially around the region of weight 0.55–0.65 pA, corresponding to a drastic change in the firing regime. In general, only 12 out of 130 cases showed an Accuracy just below 0.9. The Precision, which represents the percentage of correct detections (TP) over all those generated by the A-GLIF model (TP+FP), had a mean value of 0.852 over all simulations with at least one spike event, and was below 0.7 in only 11 out of 112 cases (see Fig. 9, top right). The Recall, which is the percentage of correct detections (TP) over all those generated by the reference model (TP+FN), had a mean value of 0.88 over all simulations with at least one spike, and it was slightly lower (0.7) for 12 out of 112 cases (see Fig. 9, bottom left). The minimum Precision and Recall values (Precision = 0.33, Recall = 0.2) occurred

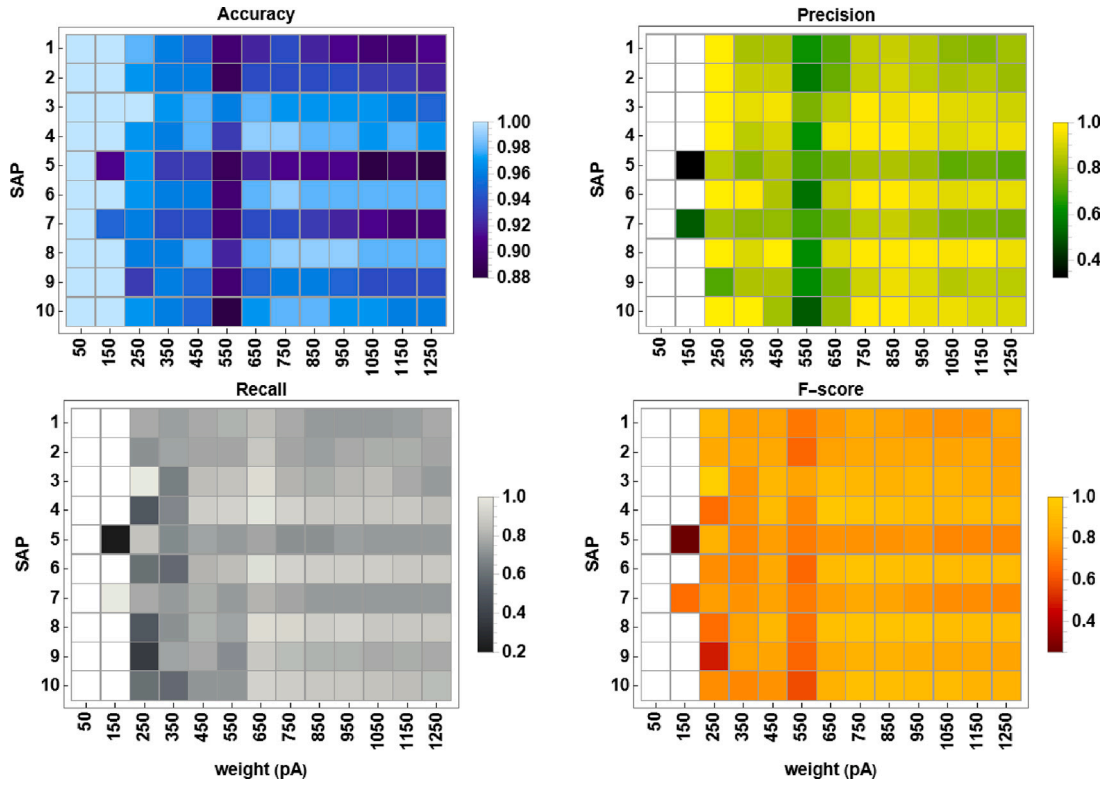

Fig. 9. Performance measures of the A-GLIF model. Accuracy (blue shades regions), precision (green shades region), recall (gray shades region), and F-score (orange shades region) for the model traces obtained in response to the 130 synaptic stimulations. White regions refer to traces without spikes both in reference and in A-GLIF models.

in the extreme case (SAP 5, weight 150 pA) where the A-GLIF model generated 3 spikes for an experimental trace with 5 spikes, resulting in only 1 TP. Finally, the F-score focuses on the correctly predicted spike times over all detected spikes and represents the harmonic mean of the Precision and Recall. Over the simulations where the F-score can be computed has a mean value of 0.811, with only 10 out of 112 cases having a value just below 0.7 (see Fig. 9, bottom right).

In Fig. 10 we show the full set of the total number of spikes generated by SAPs 4 and 8 as a function of the synaptic weight (Fig. 10, red markers and lines), compared with those obtained with the A-GLIF model (Fig. 10, blue markers and lines). Similar results were obtained in all cases, as shown for all SAPs in Fig. A.2. Typical results of somatic traces are shown in Fig. 10 (Fig. 10, insets), where we compare the traces of the reference and A-GLIF models in response to the train of synaptic inputs generated by SAPs 4 and 8 with a 650 and 850 pA peak weight, respectively. The quantitative agreement between the reference and the A-GLIF model is evident over the entire range of inputs, and these results demonstrate the ability of our model in reproducing the expected response under a large variety synaptic inputs and without the need of re-optimize the model parameters obtained using experimental traces under constant current injections.

4. Discussion

In general, the intrinsically simple mathematical structure of a model based on LIF equations can reproduce only a very limited set of experimental traces. Adapting and bursting firing patterns or depolarization blocks, very common in a number of neuron populations require GLIF models, where the LIF equations are complemented by an appropriate set of initial and update rules that must be carved to reproduce the firing patterns of the specific neuronal population of interest.

In a previous paper [13], we have considered a spiking neuron model implementation (A-GLIF) that was able to reproduce the response of several hippocampal CA1 pyramidal and interneurons during constant current step injections of different amplitude. To the best of our knowledge, this is the only model, written in terms of linear ODEs, able to quantitatively reproduce the full range of firing behavior observed experimentally in these neurons.

In this paper we solved yet another common limitation of GLIF models, namely the problem of simultaneously reproducing experimental traces obtained under constant and variable current inputs. It arises from the type of traces used to implement the update rules that, almost universally, are obtained from relatively long current steps at constant amplitudes. It should be clear that, under these conditions, the update rules will be found for constant currents; they cannot also take into account the non-linear dynamics of the membrane potential during the highly variable inputs generated by a synaptic activity. A new set of update rules thus need to be found. This was attempted in a notable previous example [11], in which the optimization procedure used a very large set of experimental traces from cortical pyramidal neurons under four different experimental protocols, including dynamic current clamp, for fitting the parameters of GLIF models. Although they obtained, in several cases, reasonable qualitative results for traces recorded under dynamic current clamp, the resulting models were not able to quantitatively reproduce experimental findings with constant (e.g. https://celltypes.brain-map.org/experiment/electrophysiology/471129934) or variable current injections (e.g. https://celltypes.brain-map.org/experiment/electrophysiology/480351780) or both (e.g. https://celltypes.brain-map.org/experiment/electrophysiology/603502705), even if they were used for the optimization process.

In this paper we solved this problem and showed how, by enriching the model with a new set of update rules, derived by analyzing the responses of a realistic neuron to in vivo-like synaptic stimulations, a model that was optimized using constant current injections was also able to predict surprisingly well the response under a barrage of synaptic inputs. This is an important issue because, in a more realistic situation, the models would be part of a very large network, where

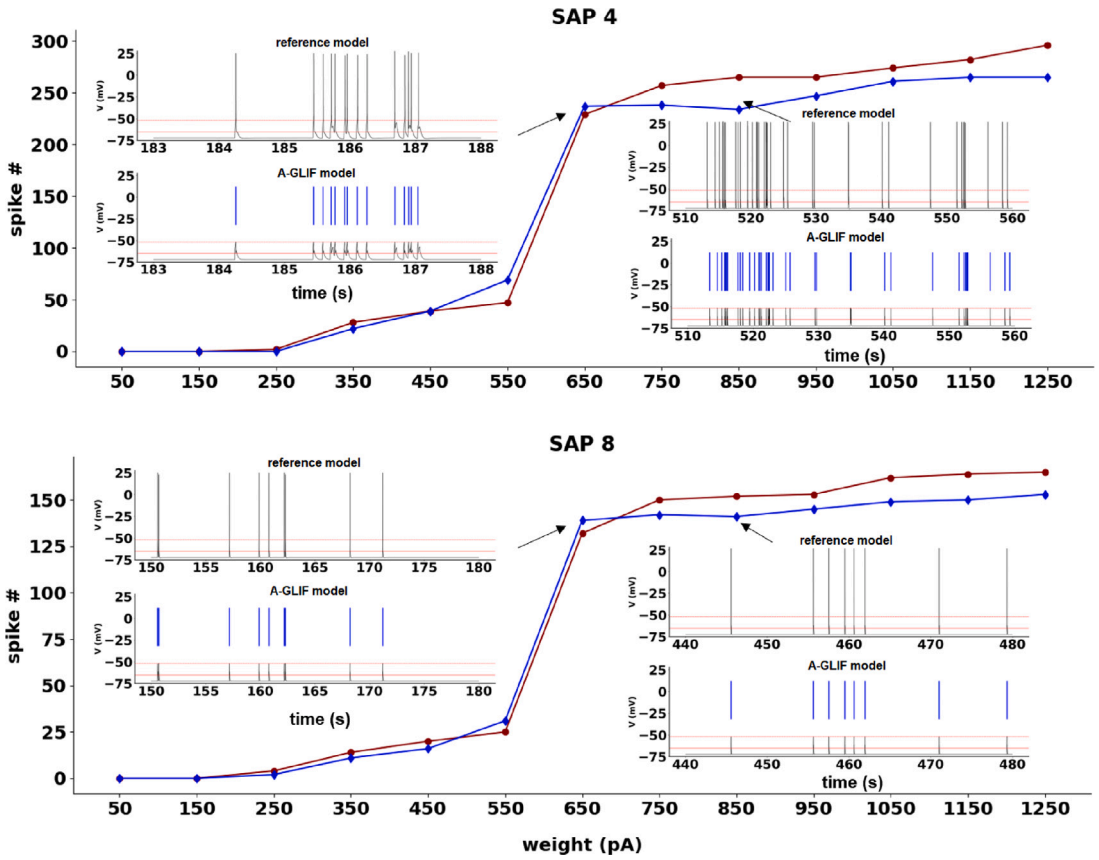

Fig. 10. Total number of spikes generated by SAPs 4 and 8 as a function of the peak synaptic weight. Red and blue symbols and lines refer to the reference and A-GLIF model, respectively. The insets show the somatic traces of the reference ("in silico" plots) and A-GLIF model ("model" plots) under the specific conditions indicated by the arrows. All performance measures calculated over the time windows shown in the insets gave values >0.88.

the input currents would be generated by an ensemble of presynaptic neurons. Alternative ways to bypass this problem, such as the ED-LUT approach [7,8], requires storing a large volume of data; here we provide a first principle approach by simplifying the model and thus minimizing the amount of information to store.

One possible limitation of our approach is that we could not validate the model against electrophysiological traces, obtained from real individual neurons in response to controlled in vivo-like synaptic inputs. Unfortunately there are no experimental data available under this condition, which is almost impossible to achieve in a laboratory. We have assumed that the use of a realistic model, although with a spatially restricted synaptic input and passive dendrites, can be a reasonable approximation that can also be used to implement models of other neuron populations.

To the best of our knowledge, this is the first time that a simplified computational model, optimized against constant current injections, is demonstrated to be universally valid for any experimental protocol (constant or variable). Any other published model based on a simplified implementation of neuronal voltage dynamics, including Izhikevic and AdEX, have not been shown to be able to quantitatively reproduce, at the same time, somatic traces in response to constant current stimulation and highly variable synaptic inputs. Instead, the results obtained with the model discussed here were statistically indistinguishable from the experimental findings not only for the stimulation protocol used for the optimization procedure (somatic constant current injections (see [13])), but also under variable current injections generated by in vivo-like synaptic inputs.

In conclusion, the high model accuracy in robustly reproducing the response to a wide variety of synaptic inputs and constant current injections, make the models obtained using the approach described here an extremely valuable tool for an efficient implementation of full-scale brain regions at cellular level.

Code availability

All model and simulation files are available in the ModelDb database (see Section 2.5).

CRediT authorship contribution statement

A. Marasco: Methodology, Funding acquisition, Supervision, Validation, Writing – original draft, Conceptualization, Formal analysis. **C. Tribuzi:** Writing – original draft, Data curation, Software. **C.A. Lupascu:** Writing – original draft, Software, Data curation. **M. Migliore:** Resources, Funding acquisition, Conceptualization, Supervision, Writing – original draft.

Declaration of competing interest

All the authors declare that no competing interests exist.

Acknowledgments

We thank the CINECA consortium (Bologna, Italy), for access to their supercomputer systems. The authors also would like to thank Sergio Solinas for support on the numerical integration of the A-GLIF model in NEST environment, and Alessia Bonafede for technical and administrative assistance.

Funding

This paper has been funded by the Italian National Recovery and Resilience Plan (NRRP), M4C2, funded by the European Union – NextGenerationEU (Project IR0000011, CUP B51E22000150006, "EBRAINS-Italy"), and by the EU Horizon Europe Program under the specific Grant Agreement 101147319, EBRAINS 2.0 project.

Appendix. Supporting information

A.1. Stability analysis of the A-GLIF model, general integral, and monotonicity properties of the membrane potential

The nondimensional version of the system (1) is

$$\begin{aligned}\frac{d\tilde{V}}{d\tilde{t}} &= \alpha + \beta(\tilde{I}_{\rm dep} - \tilde{I}_{\rm adap}) + \delta(1+\tilde{V}),\\ \frac{d\tilde{I}_{\rm adap}}{d\tilde{t}} &= 1 - \tilde{I}_{\rm adap} + \tilde{V},\\ \frac{d\tilde{I}_{\rm dep}}{d\tilde{t}} &= -\beta\tilde{I}_{\rm dep},\end{aligned} \tag{22}$$

where

$$\alpha = \frac{I_{\rm stim}}{K}, \qquad \beta = \frac{k_1}{k_2}, \qquad \delta = \frac{1}{k_2\,\tau_{\rm m}}, \qquad \tau = \frac{1}{k_2}, \qquad K = -C_m\,E_L\,k_2 \tag{23}$$

and the rescaled variables write

$$\tilde{t} = \frac{t}{\tau}, \qquad \tilde{V} = -\frac{V}{E_{\rm L}}, \qquad \tilde{I}_{\rm adap} = -\frac{I_{\rm adap}}{E_{\rm L}\,C_{\rm m}k_1}, \qquad \tilde{I}_{\rm dep} = -\frac{I_{\rm dep}}{E_{\rm L}\,C_{\rm m}k_1}. \tag{24}$$

Similarly, the dimensionless initial conditions (2) and (4) assume the following forms, respectively (for simplicity, from now on we will omit the tilde)

$$V(t_{\rm start}) = -1, \qquad V(t^+_{\rm spk}) = -\frac{V_{\rm r}}{E_{\rm L}}, \tag{25a}$$

$$I_{\rm adap}(t_{\rm start}) = 0, \qquad I_{\rm adap}(t^+_{\rm spk}) = c + \frac{a\,e^{b\,I_{\rm stim}\,(t^+_{\rm spk}-t_{\rm start})}}{d+(t^+_{\rm spk}-t_{\rm start})}, \tag{25b}$$

$$I_{\rm dep}(t_{\rm start}) = I^{\rm start}_{\rm dep}(I_{\rm stim}-I_{\rm th})\theta(I_{\rm stim}-I_{\rm th}), \qquad I_{\rm dep}(t^+_{\rm spk}) = I^0_{\rm dep}, \tag{25c}$$

where all time variables have been rescaled by means of $\tau = 1/k_2$.

In [13], assuming a *constant stimulation current* $I_{\rm stim}$, we obtained the analytical form of the solutions of the linear system (22) as follows

$$\begin{aligned}V(t) &= -I^0_{\rm adap}\beta\mathcal{H}_1 + I^0_{\rm dep}\frac{\beta\left[(\beta-1)\left(\mathcal{H}_2 - 2e^{\beta(t_0-t)}\right)\right] + \mathcal{H}_1\left[(\beta-1)(\delta+1)+2\beta\right]}{2\left(\beta^2+(\beta-1)\delta\right)}\\ &\quad + \frac{V^0}{2}\left[(\delta+1)\mathcal{H}_1+\mathcal{H}_2\right] + \frac{\mathcal{H}_1}{2}\left[\frac{\alpha(\beta-1)}{\beta-\delta}+\alpha+\delta+1\right]\\ &\quad - \frac{(\mathcal{H}_2-2)(\alpha-\beta+\delta)}{2(\beta-\delta)},\\ I_{\rm adap}(t) &= \frac{1}{2}I^0_{\rm adap}\left[\mathcal{H}_2-(\delta+1)\mathcal{H}_1\right] + I^0_{\rm dep}\frac{\beta}{2}\left[\frac{2e^{\beta(t_0-t)}+\mathcal{H}_1(2\beta+\delta-1)-\mathcal{H}_2}{\beta^2+(\beta-1)\delta}\right]\\ &\quad + V^0\mathcal{H}_1 - \frac{\alpha}{2}\left[\frac{(1-\delta)\mathcal{H}_1+\mathcal{H}_2-2}{\beta-\delta}\right] + \mathcal{H}_1,\\ I_{\rm dep}(t) &= I^0_{\rm dep}e^{-\beta(t-t_0)},\end{aligned} \tag{26}$$

where

$$V^0 := V(t_0), \quad I^0_{\rm adap} := I_{\rm adap}(t_0), \quad I^0_{\rm dep} := I_{\rm dep}(t_0). \tag{27}$$

are the initial data (25), and

$$\mathcal{A} = (\delta+1)^2 - 4\beta, \quad \mathcal{B} = -\frac{1}{2}\left(\sqrt{\mathcal{A}}-\delta+1\right)(t-t_0), \quad \mathcal{C} = \sqrt{\mathcal{A}}(t-t_0),$$

$$\mathcal{H}_1 = \frac{e^{\mathcal{B}}\left(e^{\mathcal{C}}-1\right)}{\sqrt{\mathcal{A}}}, \quad \mathcal{H}_2 = e^{\mathcal{B}}\left(e^{\mathcal{C}}+1\right). \tag{28}$$

Since $V(t)$ is an increasing function of t for any positive stimulation current $I_{\rm stim} > I_{\rm th}$, the initial data $I^0_{\rm dep}$ and $I^0_{\rm adap}$ must satisfy the following condition (see Eq. (25))

$$I^0_{\rm adap} < \frac{\alpha}{\beta} + I^0_{\rm dep} + \frac{\delta}{\beta}(1+V^0). \tag{29}$$

In the sequel we report the fundamental results of the analysis performed in [13] to determine general constraints on model's parameter. For $\alpha \neq 0$ or $\beta \neq \delta$, we impose that the (unique) equilibrium

$$E_1 = \left(\frac{\alpha}{\beta-\delta}-1,\ \frac{\alpha}{\beta-\delta},\ 0\right), \tag{30}$$

is (globally) asymptotically stable, i.e.,

$$\delta < \beta \le \frac{1}{4}(1+\delta)^2 \quad \text{with } 0<\delta<1. \tag{31}$$

Furthermore, by imposing that the cell will not fire for $0 < I_{\rm stim} < I_{\rm th}$ we obtain

$$\alpha_{\rm th} < \frac{(1+V_{\rm th})(\delta-1)^2}{4}, \quad \frac{\alpha_{\rm th}}{1+V_{\rm th}} + \delta < \beta \le \frac{1}{4}(\delta+1)^2, \quad 0<\delta<1, \tag{32}$$

where $\alpha_{\rm th} = I_{\rm th}/K$.

Finally, under the constraints (31), we proved the following monotonicity properties of the potential V (see [13,14])

$$\begin{aligned}\frac{dV}{d\alpha} &= \frac{2-\mathcal{H}_1(1-2\beta+\delta)-\mathcal{H}_2}{2(\beta-\delta)} > 0,\\ \frac{dV}{dI^0_{\rm adap}} &= -\beta\,\mathcal{H}_1 < 0\\ \frac{dV}{dI^0_{\rm dep}} &= \frac{\beta\left[\left(\mathcal{H}_2 - 2e^{-\beta(t-t_0)}+\mathcal{H}_1(1+\delta)\right)(\beta-1)+2\beta\mathcal{H}_1\right]}{2\left[\beta^2+(\beta-1)\delta\right]} > 0.\end{aligned} \tag{33}$$

A.2. Updates rules for constant and piecewise constant stimulation currents

In [13], to obtain a model able to accurately reproduce the spike times in response to any constant and piecewise constant stimulation currents, the following updates rules are introduced

1. For a positive stimulation outside the experimentally tested range, i.e. $I_{\rm th} < I_{\rm stim} < I^{\rm min}_{\rm stim}$ or $I_{\rm stim} > I^{\rm max}_{\rm stim}$, the sequence of initial data $I^0_{\rm adap}(t^+_{\rm spk}, I_{\rm stim})$ in Eq. (25) may contain negative values, as shown in Fig. A.1 (gray dots and lines). In these cases, it is sufficient to translate the Monod function along the vertical axis as follows (see [13] and Fig. A.1)

$$\left(I^0_{\rm adap}(t^+_{\rm spk}, I_{\rm stim})\right)^* := c^* + \frac{a\,e^{b\,I_{\rm stim}}(t^+_{\rm spk}-t_{\rm start})}{d+(t^+_{\rm spk}-t_{\rm start})}, \tag{34}$$

where

$$c^* := \begin{cases} c-L, & \text{if } a>0,\\ -a\,e^{b\,I_{\rm stim}}, & \text{if } a<0,\end{cases} \tag{35}$$

and $L = I^0_{\rm adap}(t^{\rm first}_{\rm spk}\left(I_{\rm stim}\right), I_{\rm stim}) < 0$.
In particular, we adopt the function (34) after detecting negative values of $I^0_{\rm adap}$ twice (see the right panel in Fig. A.1).

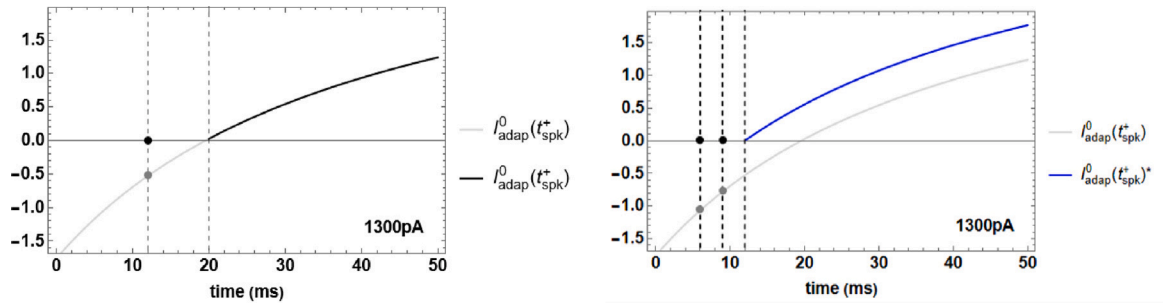

Fig. A.1. Monod-type function for $I_{stim} = 1300$ pA is analyzed in two scenarios. The vertical dashed lines represent the time instants t^+_{spk} in which to evaluate the values of I^0_{adap} on the Monod function (25). (left) At the first time instant the value of I^0_{adap} on the Monod function (25) is negative (gray dot), then we set this value to zero (blach dot), while from the second time instant onwards the Monod function remains nonnegative (black line) and no further changes are necessary. (right) As for the first panel for the first two time instants (gray dots), at the third time instant the Monod function (25) is still negative (gray line), therefore we substitute it with the function in Eq. (34) (blue line) obtained through a translation of $-L$ along the vertical axis.

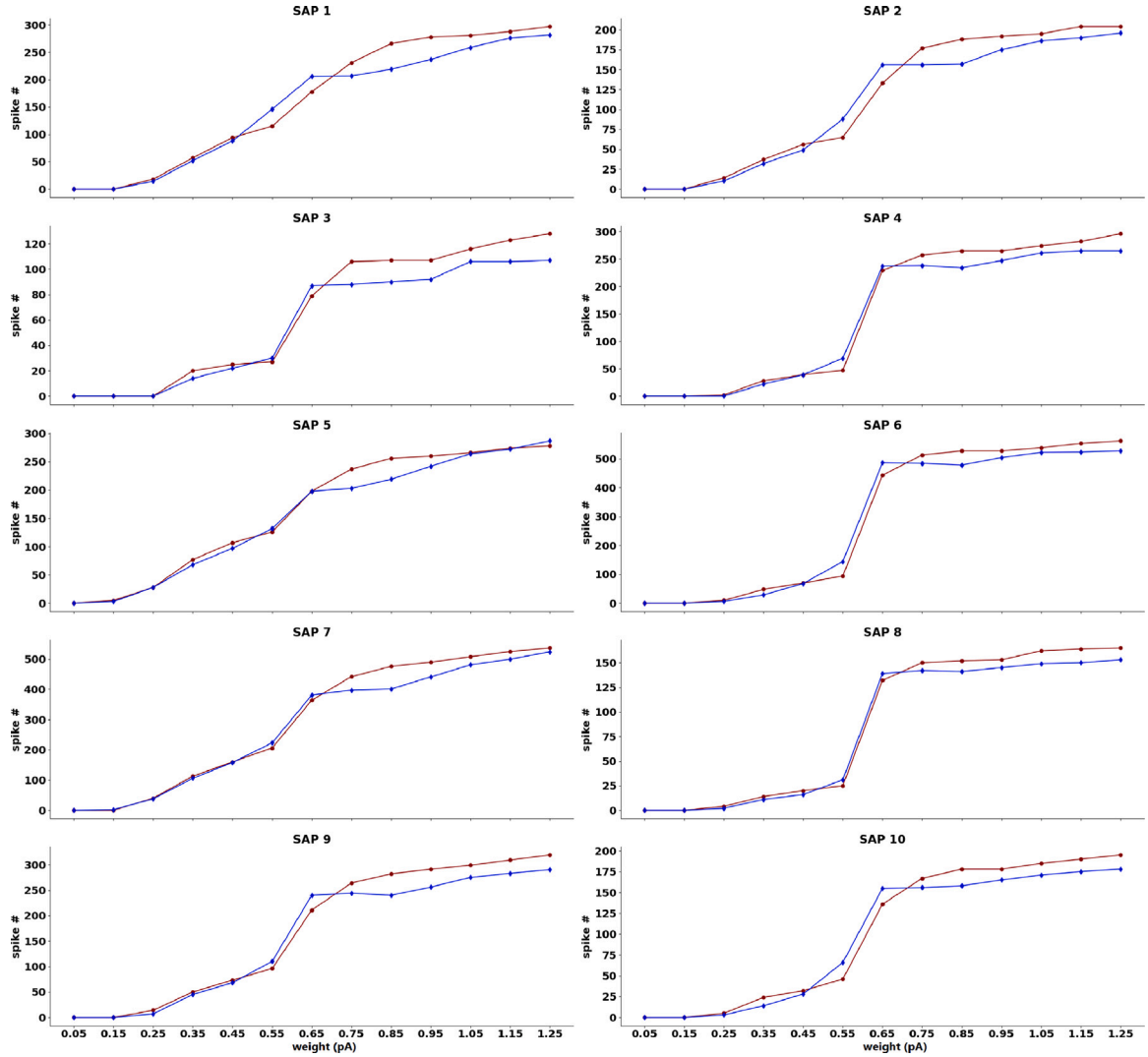

Fig. A.2. Total number of spikes generated by all SAPs as a function of the peak synaptic weight. Red and blue symbols and lines refer to the reference and A-GLIF models, respectively.

2. Let t be a time such that $I_{th} < I_{stim}(t) < I_{stim}(t - dt)$ and $t < t_{block}(I_{stim}(t))$. From a physiological point of view, the only constraint for the model after such a change in the current is that the membrane voltage should still be increasing, albeit more slowly, i.e. $\dot{V}(t) > 0$. Considering Eq. $(22)_1$ and Eq. (29), this condition can be obtained by setting the initial condition for V,

Table A.1
P-values of the Mann–Whitney U-test. The missing values refer to paired data containing fewer than 10 spike times.

SAP	Weight (pA)												
	50	150	250	350	450	550	650	750	850	950	1050	1150	1250
1	–	–	0.44	0.98	0.92	0.86	0.74	0.88	0.72	0.55	0.75	0.89	0.86
2	–	–	0.43	0.90	0.40	0.36	0.79	0.69	0.90	0.92	0.80	0.79	0.98
3	–	–	–	0.77	0.6	0.45	0.81	0.85	0.95	0.77	0.98	0.99	0.99
4	–	–	–	0.63	0.89	0.87	0.77	0.87	0.99	0.90	0.95	0.88	0.89
5	–	0.77	0.61	0.60	0.79	0.57	0.67	0.69	0.77	0.76	0.44	0.56	0.40
6	–	–	–	0.33	0.85	0.66	0.69	0.99	0.98	0.78	0.93	0.85	0.99
7	–	–	0.91	0.83	0.62	0.86	0.78	0.58	0.78	0.94	0.96	0.78	0.75
8	–	–	–	0.93	0.67	0.53	0.81	0.87	0.79	0.97	0.97	0.95	0.85
9	–	–	–	0.75	0.56	0.22	0.74	0.99	0.89	0.99	0.96	0.85	0.76
10	–	–	–	0.84	0.99	0.99	0.91	0.86	0.91	0.92	0.83	0.91	0.61

I_{dep}, and I_{adap} as follows (see [13] for more details)

$$V^0(t) = V(t), \quad I^0_{\text{adap}}(t) = I_{\text{adap}}(t), \quad I^0_{\text{dep}}(t) = I^0_{\text{adap}}(t) + \Theta^\star \frac{\alpha}{\beta}, \tag{36}$$

where the constant $\Theta^\star$ is defined as

$$\Theta^\star = \begin{cases} \Theta & \text{if } \Theta \geq 0, \\ 0 & \text{if } \Theta < 0, \end{cases} \tag{37}$$

where

$$\Theta = \frac{V(t-dt)}{\bar{\alpha}} \left(\frac{1}{dt} - \delta \right) - \frac{V(t-2dt)}{\bar{\alpha} dt} - \frac{\delta}{\bar{\alpha}} - 1, \tag{38}$$

and $\bar{\alpha} = I_{\text{stim}}(t-dt)/K$, with K defined in Eq. (24).

3. If the current increases at t, i.e. $I_{\text{stim}}(t) > I_{\text{stim}}(t-dt) > I_{\text{th}}$ and $t < t_{\text{block}}(I_{\text{stim}}(t))$, then the system just continues with its dynamics, with initial conditions thus updated as

$$V^0(t) = V(t), \quad I^0_{\text{adap}}(t) = I_{\text{adap}}(t), \quad I^0_{\text{dep}}(t) = I_{\text{dep}}(t). \tag{39}$$

A.3. Supplementary tables, and figures

See Table A.1 and Fig. A.2.

References

[1] Cheng Ly, Firing rate dynamics in recurrent spiking neural networks with intrinsic and network heterogeneity, J. Comput. Neurosci. 39 (3) (2015) 311–327.

[2] Tadashi Yamazaki, Jun Igarashi, Realtime cerebellum: A large-scale spiking network model of the cerebellum that runs in realtime using a graphics processing unit, Neural Netw. 47 (2013) 103–111.

[3] R. Brette, W. Gerstner, Adaptive exponential integrate-and-fire model as an effective description of neuronal activity, J. Neurophysiol. 94 (5) (2005) 3637–3642.

[4] T. Górski, D. Depannemaecker, A. Destexhe, Conductance-based adaptive exponential integrate-and-fire model, Neural Comput. 33 (1) (2021) 41–66.

[5] Eugene M. Izhikevich, Gerald M. Edelman, Large-scale model of mammalian thalamocortical systems, Proc. Natl. Acad. Sci. 105 (9) (2008) 3593–3598.

[6] Gabriel Marghoti, Thiago de Lima Prado, Arturo Cagnato Conte, Fabiano Alan Serafim Ferrari, Sergio Roberto Lopes, Intermittent chimera-like and bi-stable synchronization states in network of distinct izhikevich neurons, Chaos Solitons Fractals 162 (2022) 112401.

[7] E. Ros, R. Carrillo, E.M. Ortigosa, B. Barbour, R. Agís, Event-driven simulation scheme for spiking neural networks using lookup tables to characterize neuronal dynamics, Neural Comput. 18 (12) (2006) 2959–2993.

[8] R. Carrillo, E. Ros, S. Tolu, T. Nieus, E. D'Angelo, Event-driven simulation of cerebellar granule cells, Biosystems 94 (2008) 10–17.

[9] N.D. Jimenez, S. Mihalas, R. Brown, E. Niebur, J. Rubin, Locally contractive dynamics in generalized integrate-and-fire neurons, SIAM J. Appl. Dyn. Syst. 12 (3) (2013) 1474–1514.

[10] A. Geminiani, C. Casellato, F. Locatelli, F. Prestori, A. Pedrocchi, E. D'Angelo, Complex dynamics in simplified neuronal models: Reproducing golgi cell electroresponsiveness, Front. Neuroinform. 12 (2018).

[11] C. Teeter, R. Iyer, V. Menon, N. Gouwens, D. Feng, J. Berg, A. Szafer, N. Cain, H. Zeng, M. Hawrylycz, C. Koch, S. Mihalas, Generalized leaky integrate-and-fire models classify multiple neuron types, Nature Commun. 9 (1) (2018).

[12] Z. Wang, L. Guo, M. Adjouadi, A generalized leaky integrate-and-fire neuron model with fast implementation method, Int. J. Neural Syst. 24 (05) (2014) 1440004.

[13] A. Marasco, E. Spera, V. De Falco, A. Iuorio, C.A. Lupascu andS. Solinas, M. Migliore, An adaptive generalized leaky integrate-and-fire model for hippocampal CA1 pyramidal neurons and interneurons, Bull. Math. Biol. 85 (11) (2023) 109.

[14] A. Marasco, C. Tribuzi, A Iuorio, M. Migliore, Mathematical generation of data-driven hippocampal CA1 pyramidal neurons and interneurons copies via A-GLIF models for large-scale networks covering the experimental variability range, Math. Biosci. 371 (2024) 109179.

[15] M.L. Hines, N.T. Carnevale, The NEURON simulation environment, Neural Comput. 9 (6) (1997) 1179–1209.

[16] Rosanna Migliore, Carmen A. Lupascu, Luca L. Bologna, Armando Romani, Jean-Denis Courcol, Stefano Antonel, Werner A. H. Van Geit, Alex M. Thomson, Audrey Mercer, Sigrun Lange, Joanne Falck, Christian A. Rössert, Ying Shi, Olivier Hagens, Maurizio Pezzoli, Tamas F. Freund, Szabolcs Kali, Eilif B. Muller, Felix Schürmann, Henry Markram, Michele Migliore, The physiological variability of channel density in hippocampal CA1 pyramidal cells and interneurons explored using a unified data-driven modeling workflow, in: William W. Lytton (Ed.), PLOS Comput. Biol. 14 (9) (2018) e1006423.

[17] Michele Migliore, Giorgio A. Ascoli, David B. Jaffe, CA3 cells: Detailed and simplified pyramidal cell models, in: Vassilis Cutsuridis, Bruce Graham, Stuart Cobb, Imre Vida (Eds.), Hippocampal Microcircuits: A Computational Modeler's Resource Book, Springer New York, New York, NY, 2010, pp. 353–374.

[18] R. Migliore, G. De Simone, X. Leinekugel, M. Migliore, The possible consequences for cognitive functions of external electric fields at power line frequency on hippocampal CA1 pyramidal neurons, Eur. J. Neurosci. 45 (8) (2017) 1024–1031.

[19] Samuel Garcia, Alessio P. Buccino, Pierre Yger, How do spike collisions affect spike sorting performance? eNeuro 9 (5) (2022).

[20] Evangelia I. Zacharaki, Iosif Mporas, Kyriakos Garganis, Vasileios Megalooikonomou, Spike pattern recognition by supervised classification in low dimensional embedding space, Brain Inform. 3 (2) (2016) 73–83.

[21] Catherine S. Cutts, Stephen J. Eglen, Detecting pairwise correlations in spike trains: An objective comparison of methods and application to the study of retinal waves, J. Neurosci. 34 (43) (2014) 14288–14303.

[22] M. Ciba, T. Isomura, Y. Jimbo, A. Bahmer, C. Thielemann, Spike-contrast: A novel time scale independent and multivariate measure of spike train synchrony, J. Neurosci. Methods 293 (2018) 136–143.

[23] E. Satuvuori, M. Mulansky M, N. Bozanic, I. Malvestio, F. Zeldenrust, K. Lenk, T. Kreuz, Measures of spike train synchrony for data with multiple time scales, J. Neurosci. Methods 287 (2017) 25–38.